The International Journal of Advanced Manufacturing Technology (2020) 110:2049–2066
https://doi.org/10.1007/s00170-020-05993-5

ORIGINAL ARTICLE

Selective laser sintering of carbon fiber–reinforced PA12: Gaussian process modeling and stochastic optimization of process variables

Tiago Czelusniak[1] · Fred L. Amorim[1]

Received: 26 June 2020 / Accepted: 21 August 2020 / Published online: 1 September 2020
© Springer-Verlag London Ltd., part of Springer Nature 2020

Abstract
This work presents an in-depth investigation of the influence of the individual laser sintering parameters on density, mechanical, and dimensional properties of carbon fiber–reinforced PA12 parts manufactured by selective laser sintering (SLS) . A space-filling design of experiments method was used to plan the experiments and SLS trials were conducted to manufacture test samples that were characterized in terms of dimensional accuracy, density, and mechanical properties. Gaussian process–supervised learning was used to model the interaction between laser sintering parameters and quality properties. Stochastic optimization via evolutionary algorithm was employed to obtain trade-off solutions for several multi-objective optimization tasks. The Gaussian process presented excellent model quality for the majority of response variables evaluated. Laser sintering parameters had a significant influence on physical and mechanical properties, exhibiting complex and non-linear behavior. Multi-objective optimization showed a wide range of optimized laser sintering parameters available, depending on the trade-off objective desired.

Keywords Powder bed fusion · Selective laser sintering · Gaussian process · supervised learning · Evolutionary algorithm · Polymer composites · Carbon fiber · reinforced PA12 composite

1 Introduction

Selective laser sintering (SLS) is a powder bed fusion additive manufacturing (AM) process able to fabricate three-dimensional (3D) objects layer-by-layer according to their CAD models. Powder consolidation is obtained by selectively fusing or melting the layer of loose powder using the thermal energy of one or more lasers [1, 2]. Compared to other AM techniques, SLS does not require any tooling or a support structure, being able to rapidly produce parts with highly controllable intricate internal and external structures. The complex laser–material interaction and consolidation mechanism occurring in SLS limit the range of materials available to date [3, 4]. By far, polyamide 12 (PA12) is the most commercially used and scientifically researched material due to its easier processability by SLS [5], accounting for the majority of the SLS market and providing the most relevant information for the current market.

SLS parts made with composite materials such as polymer matrix with inorganic fillers are being increasingly studied by the research community [6]. The primary purpose of this approach is to improve the mechanical properties of the material, which cannot be achieved by using a single material in its composition [7]. One of the materials recently receiving attention for SLS of end-user parts is carbon fiber–reinforced polyamide (PA12-CF). The powder form of PA12-CF is composed of PA12 spherical particles mixed with high aspect ratio carbon short fibers. The fibers receive a chemical treatment to improve the adhesion between the fibers and the polymeric matrix. Yan et al. [8] prepared carbon fibers by surface modification to improve interface adhesion with PA12 and further mixing CF with PA12 by a dissolution-precipitation method. Mechanical properties were greatly enhanced by the preparation method when compared to pure PA12. Bai et al. [9] showed that the melting pool generated during SLS of carbon nanotubes and PA12 is wider and deeper than pure PA12. More recently, carbon fiber surface modification via HNO_3 treatment was performed to improve

✉ Fred L. Amorim
fred.amorim@pucpr.br

[1] Mechanical Engineering Graduate Program, Pontificia Universidade Catolica do Parana - PUCPR, Av. Imaculada Conceição, 1155 - Prado Velho, 80, Curitiba 215 901, Brazil

www.manaraa.com

adhesion with PA12 via direct mixing [10]. Improved mechanical properties were obtained after surface modification of CFs but only when treated in a nitrogen atmosphere. The porosity of mechanically mixed PA12-CF samples manufactured in different building directions was studied employing computed tomography [11]. Highly porous structures were observed, concentrated between the layers manufactured, leading to anisotropic mechanical properties. The fracture mechanism of PA12-CF material processed by SLS was recently studied [12]. Crack growth was found to initiate at the interface between carbon fiber and PA12. Carbon nanotubes have been added to PA12 to improve mechanical behavior, reporting a significant increase in mechanical properties when compared to pure PA12 [13, 14]. Espera et. al. mechanically mixed carbon black with PA12, improving mechanical and electrical properties with an optimal filler content of 1.5% [15]. Carbon black PA12 was prepared via a two-step approach to produce SLS parts with improved electrical properties [16]. Zhu et al. [17] proposed a novel method to prepare carbon-fiber-PA12-epoxy ternary composites. The authors infiltrated the green porous PA12-CF structure with thermosetting epoxy resin, which was subsequently cured to obtain the ternary composite. The novel method reported yielded a tensile strength of 101 MPa, a significant improvement compared to pure PA12 and also to other PA12-CF composites processed by SLS.

As detailed in the literature review, most of the research carried out so far in laser sintering of PA12-CF materials was focused on material aspects, without taking into consideration the influence of the individual laser sintering parameters on quality properties. The SLS process parameters are related to the energy delivered to the powder bed and influence important quality factors such as the dimensional, surface, and mechanical properties of SLS parts. Typical process parameters include laser power, laser speed, scan line spacing, layer thickness, pre-heating temperature, and part orientation. To the authors' knowledge, no research has been conducted to investigate the effect of individual laser sintering parameters on the quality properties of SLS PA12-CF parts. Therefore, the main contribution of this research study is to investigate and optimize the influence of the individual laser sintering parameters on critical quality criteria such as surface properties, dimensional accuracy, density, and mechanical properties. To support the study, a space-filling design of experiments (DOE) is applied to conduct the experimental trials, and the influence of the individual laser sintering parameters on critical quality criteria such as dimensional accuracy, density, and mechanical properties is modeled employing Gaussian process (GP)–supervised learning. Stochastic optimization via evolutionary algorithm (EA) is applied to perform multi-objective optimization tasks for different criteria.

2 Materials and methods

2.1 Materials

The material studied was carbon fiber–reinforced PA12 (PA12-CF), which is a commercially available material (commercially known as CarbonMide, from EOS manufacturer) for laser sintering applications [18], composed by PA12 and anthracite black carbon fiber PA12-CF powder. SEM micrographs of the described powder at × 200 and × 1000 magnification are depicted in Fig. 1. As observed from the micrographs, carbon fibers are uniformly dispersed along with the "potato-shaped" PA12 polymer particles.

2.2 SLS processing and design of experiments

An EOS P396 laser sintering machine was used to perform the SLS experiments, equipped with a 70 W continuous-wave Gaussian CO_2 laser (wavelength 10.6 μm) and a laser spot diameter of 0.5 mm. Standard dumbbell-shaped type I (ASTM Standard D638-02a, 2002 [19]) and rectangular (ASTM Standard D790-02,2002 [20]) samples were manufactured. All samples were positioned in the building platform *X*-direction (the same direction as the recoater blade moving direction) and using an alternate *x*–y scanning pattern. The parts were placed as close as possible to the center of the building platform to minimize the effects of non-uniform powder temperatures on the building platform. In order to evaluate the influence of the individual laser sintering parameters, laser power, laser scan speed, and scan line spacing were varied using a Sobol space-filling DOE methodology, which has the advantage of best design space coverage and uniformity [21]. Twenty-four laser parameter sets were defined, with laser power varying from 30 to 45 W, laser scan speed from 2000 to 5000 mm/s, and scan line spacing from 0.2 to 0.6 mm. The layer thickness was fixed at 150 μm. Figure 2 shows the design space covered by the Sobol space DOE. Table 1 shows the experimental design matrix. The pre-heating temperature was kept at 178 °C during all laser sintering process. For each parameter combination, 5 dumbbell and 5 rectangular samples were produced, giving a total of 240 samples evaluated.

2.3 Response surface modeling—Gaussian process–supervised learning

Response surface modeling (RSM) is adopted to model the influence of the laser sintering variables on response variables. The goal is to use the results from the DOE run in order to create an empirical model of the response variables over the design space. In a more general way, this approach concerns supervised learning, which consists of learning the mapping between input and output variables from empirical data (training data). RSM using supervised learning is very useful to

www.manaraa.com

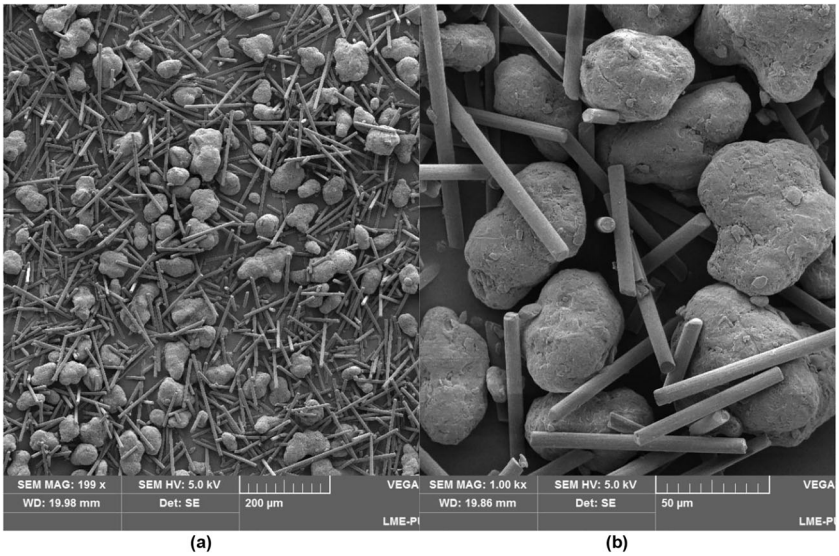

Fig. 1 Powder images from scanning electron microscope (SEM) depicting PA12-CF

predict the behavior of response variables and provide a set of parameters yielding optimal response, which are the main objectives of this study.

Traditional RSM methods include the least square method and polynomial fit (linear, quadratic, cubic). Such methods make assumptions about the characteristics of the underlying function $f(x)$. For instance, if the behavior of the output at given inputs is linear, it is reasonable to assume a linear regression model. The main drawback of such approaches is the limited flexibility involved, as the prior assumption of the underlying function can give poor prediction results if the relationship between input and output cannot be reasonably approximated by the given function. Another approach is to give a prior probability to every possible function considered more likely. This function probability is precisely what Gaussian process (GP) aims. Unlike polynomial methods, GP does not claim specific functions relating to the data, being a less parametric tool [22]. Given a training dataset (collection of inputs and outputs), a GP will infer the most likely functions that pass through the observed data. This method uses no descriptive model based on physical processes, being deduced statistically from measured data only [21]. GP can be described as a distribution over functions and inference taking place directly in the space of functions.

More specifically, a GP is a collection of random variables which is described by its mean function $m(x)$ and covariance function $k(x, x')$. A GP is defined by equation 1.

$$\begin{aligned} m(x) &= E[f(x)] \\ k\left(x,x'\right) &= E\left[\left(f(x)-m(x)\right)\left(f\left(x'\right)-m\left(x'\right)\right)\right] \\ f(x) &\sim \mathrm{GP}\left(m(x), k\left(x,x'\right)\right) \end{aligned} \tag{1}$$

A GP is a probability distribution over possible functions. Random variables represent the value of function $f(x)$ at

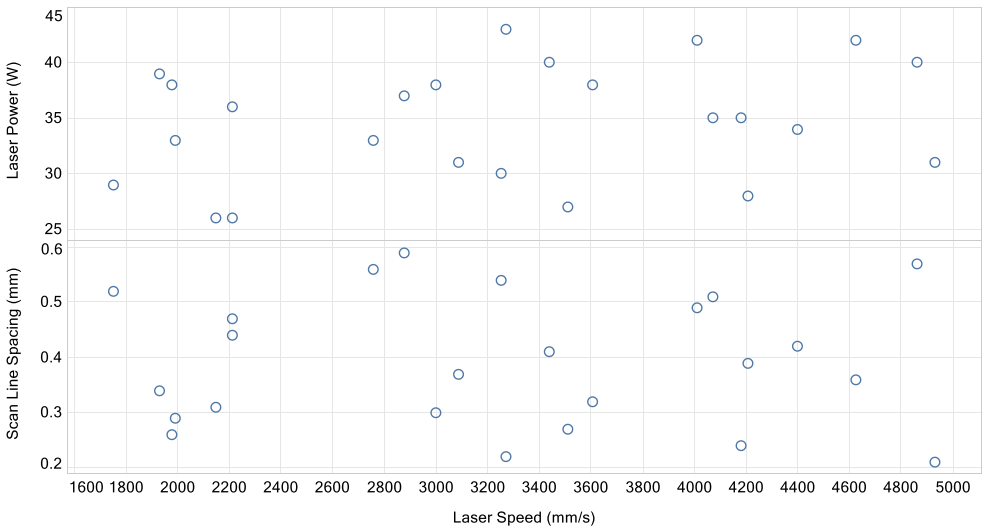

Fig. 2 Laser sintering parameters design space covered by Sobol space-filling DOE

www.manaraa.com

Table 1 Experimental design matrix

Experiment_Id	Laser power (W)	Laser Speed (mm/s)	Scan Line Spacing (mm)
1	26	2212	0.44
2	35	4180	0.24
3	39	1929	0.34
4	30	3251	0.54
5	33	1992	0.29
6	42	4010	0.49
7	37	2876	0.59
8	28	4206	0.39
9	29	1751	0.52
10	38	3607	0.32
11	43	3271	0.22
12	34	4398	0.42
13	31	3086	0.37
14	40	4862	0.57
15	36	2211	0.47
16	27	3511	0.27
17	26	2149	0.31
18	35	4070	0.51
19	40	3438	0.41
20	31	4931	0.21
21	33	2758	0.56
22	42	4625	0.36
23	38	1978	0.26
24	38	3000	0.3

location x, while the covariance function (kernel function) specifies the covariance between pairs of random variables $f(x)$ and $f(x')$, which measure the similarity between points and give important properties of functions such as smoothness and stationarity. The mean function $m(x)$ represents the expectation E of $f(x)$.

This work proposes, for the first time, the use of GP to perform the RSM of the SLS process variables. GP method is known to achieve a good approximation of response surfaces and improved optimization results, being often used in machine learning tasks. Also, GP gives a good prediction of variance, which measures the uncertainty of the model. The squared exponential function was used as the covariance function, which is known to give smoother models [22]. The squared exponential covariance function is defined by equation 2.

$$k\left(x,x'\right) = \sigma^2 \exp\left(-\frac{\left(x-x'\right)^2}{2l_c^2}\right) \tag{2}$$

where x and x' are neighboring input values. $f(x)$ and $f(x')$ are the modeled outputs at the given input values. The hyperparameter σ is defined as the variance of the response variable, and l_c is defined as the characteristic length scale of the covariance function. The covariance function between outputs is described in terms of their respective inputs. It can be seen that the covariance function is close to σ^2 at variables whose corresponding inputs are very close, decreasing as the distance between the inputs increases. The GP modeling for laser sintering parameters used a Matlab implementation of GP models publicly available [23].

The following quality response variables were evaluated and modeled using GP:

- X-direction dimensional accuracy (same direction as the recoater blade moving direction)
- Y-direction dimensional accuracy (direction perpendicular to the recoater blade moving direction)
- Z-direction dimensional accuracy (same direction as the building direction)
- Apparent density
- Average surface roughness (R_a)
- Tensile strength at yield
- Nominal strain at break
- Elastic modulus
- Normalized manufacturing time

www.manaraa.com

The model quality for each response variable was evaluated through plots of prediction and measured data and statistical quality criteria such as root mean square error (RMSE) to check the absolute error measure, and the coefficient of determination R^2 to check the portion of the total variance of the measuring data is described by the model. RMSE and R^2 are given by equations 3 and 4, respectively.

$$\mathrm{RMSE} = \sqrt{\frac{\sum_{i=1}^{n}\left(y_{i,\mathrm{pred}} - y_{i,\mathrm{meas}}\right)^2}{n}} \tag{3}$$

$$R^2 = 1 - \frac{\sum_{i=1}^{n}\left(y_{i,\mathrm{pred}} - y_{i,\mathrm{meas}}\right)^2}{\sum_{i=1}^{n}\left(y_{i,\mathrm{meas}} - \overline{y}_{\mathrm{meas}}\right)^2} \tag{4}$$

where $y_{i,\ \mathrm{pred}}$ is the modeled output of a response variable at a given input, $y_{i,\ \mathrm{meas}}$ is the measured value of a response variable at the same input, and $\overline{y}_{\mathrm{meas}}$ is the average value of all the measured data of the respective response variable. For both measures, the leave one out cross-validation (LOOCV) was applied, i.e., one point of the training data was left out as validation data, the model was trained, and the error of the one data point which was not used in the model training was calculated. The procedure was repeated until each data point was used once for validation, and the overall validation error was evaluated in terms of RMSE and R^2. Models with $R^2 \geq 0.9$ were considered excellent and suitable for quantitative predictions; Models with $0.6 < R^2 < 0.9$ were considered of intermediate quality and suitable for qualitative analysis; models with $R^2 \leq 0.6$ were considered not reliable. Only models with $R^2 > 0.6$ were considered for further analysis of response functions, as a qualitative analysis can be performed, and useful information can be derived even from models with intermediate quality. Only models with $R^2 \geq 0.9$ were considered for further optimization tasks.

2.4 Evolutionary algorithm stochastic optimization

The results derived from GP modeling were further used to perform optimization tasks with distinct objectives. Evolutionary algorithm (EA) stochastic optimization was employed to perform the optimization tasks. EA was chosen as the optimization method as it performs well under a wide range of higher dimensional problems and is robust against noisy evaluation functions [24]. EA aims at simulating the evolution of a population through successive generations of better performing individuals. By applying mutation operators on previous generations, a new generation is created, evaluated for fitness, and selected. The steps are repeated until the termination criteria are achieved [24]. The main steps in EA optimization are as follow:

1. Initialization: the first population of individuals is randomly created.
2. Mutation: a mutant individual is created for each individual in the population.
3. Cross-over: the mutant individual is combined with its parent to create a trial individual.
4. Evaluation: the fitness of the trial individual is evaluated
5. Selection: the best between trial and parent individual is selected based on the fitness function and survive to the next generation.
6. Repetition: steps 2–5 are repeated until the desired number of iterations is achieved.

Multi-criteria optimization was employed to perform the optimization tasks. Unlike single criteria optimization, where only one objective function is to be minimized or maximized, multi-criteria optimization relies on optimization of two or more objective functions. The results are not a single optimum of the functions. Instead, due to conflicting objectives, the results of a multi-criteria optimization are solution sets representing a compromise (trade-off) between the objectives. These trade-off solutions are called Pareto solutions.

Although EA is a powerful optimization tool, it has some drawbacks. The main constraints related to EA and most of stochastic optimization methods are their slow convergence towards the optimal solution or solutions and the reproducibility of the results due to the stochastic nature of these algorithms. Nevertheless, EA is known to perform well in multi-objective tasks and therefore was chosen as the optimization technique in this study [24].

Multi-criteria optimization considered mechanical properties, surface roughness, dimensional accuracy, and manufacturing time. The optimization was only performed if the GP model quality achieved was adequate for the specific response variable. Two objectives were optimized at once, while the others were kept at a limit (lower or upper hard limit) to reduce the number of Pareto solutions. Hard lower limit implies that solutions achieved with values below this threshold are not considered in the optimization, whereas the hard upper limit means no consideration of solutions with values above this threshold. The different scenarios considered in the multi-criteria optimization are summarized in Table 2.

For each optimization criterion, a group of Pareto solutions was chosen to identify the laser sintering parameters associated with the specific solution set.

2.5 Mechanical analysis

Force displacement measurements were performed in an EMIC DL500 mechanical testing machine. Tensile tests were conducted according to ASTM Standard D638-02a [19]. Dumbbell-shaped tensile specimens type I having dimensions of 165 × 19 × 3.2 mm were tested under a displacement rate of

www.manaraa.com

Table 2 Optimization criteria for PA12-CF response variables

Criteria	Mechanical properties	Surface roughness	Manufacturing time	Dimensional accuracy
1	Hard lower limit	Hard upper limit	*Minimize*	*Maximize*
2	Hard lower limit	*Minimize*	Hard upper limit	*Maximize*
3	*Maximize*	Hard upper limit	Hard upper limit	*Maximize*
4	Hard lower limit	*Minimize*	*Minimize*	Hard lower limit
5	*Maximize*	*Minimize*	Hard upper limit	Hard lower limit
6	*Maximize*	Hard upper limit	*Minimize*	Hard lower limit

5 mm/min. For statistical relevance, 5 samples were manufactured for each parameter set.

2.6 Dimensional, density, and surface roughness measurements

Dimensional accuracy measurements were conducted according to ASTM Standard D5947-11 [25]. Width and thickness measurements were performed using a micrometer, and a caliper was used to measure the specimen's length. The resulting data was used to calculate the volume of the rectangular samples and to further estimate the apparent density of the samples by measuring their mass with a precision balance. Surface roughness was measured with a Mahr Perthen Perthometer S8P with a cut-off length of 8 mm.

2.7 Manufacturing time calculation

Manufacturing time was evaluated using the calculations performed by the machine software. A reference manufacturing time was used based on the calculation of the manufacturing time of one tensile test sample produced with standard laser sintering parameters (parameter set *PA2200 balance* according to the machine manufacturer manual). The normalized manufacturing time θ was calculated based on the ratio between the manufacturing time calculated for the same sample at the same position but with the parameter set resulting from the DOE and the reference manufacturing time. The normalized manufacturing time is given by equation 5.

$$\theta = \frac{\text{Current Manufacturing time}}{\text{Reference manufacturing time}} \tag{5}$$

3 Results and discussion

3.1 Model quality

Table 3 presents a summary of RMSE and R^2 for each response function. *X*-direction accuracy shows very low values of R^2, and the model is not reliable. The reason for the low model quality is the small sensitivity of the output variable to the input variables. *Y*-direction accuracy has better model quality (RMSE = 0.0128; R^2 = 0.74) and suitable for qualitative assessment. *Z*-direction accuracy model quality achieved very good results (RMSE = 0.0172; R^2 = 0.93) and can be used for quantitative assessment.

Density model quality shows a good fit with the experimental data, with an R^2 of 0.85, which can be used for qualitative predictions. The surface roughness model quality is very poor (R^2 = 0.3) and cannot be considered reliable. The main reason for low model quality is the high variance of measurements performed (very noisy results) due to the nature of laser-sintered samples and also the measurement method applied, which used profile measurement. Also, there is little or no influence of the parameters evaluated on surface roughness.

Mechanical properties reached excellent model quality. Tensile strength at yield reached low RMSE and high R^2 of 0.96. Elastic modulus also achieved a very good correlation and is suitable for quantitative assessment. Regarding strain, GP model training for nominal strain at break resulted in good model quality, with low RMSE and high R^2 of 0.92.

Normalized manufacturing time is also very well represented by the GP model, mainly due to the zero variance between samples processed, as the manufacturing time is calculated based on the machine's parameters.

Table 3 GP response functions model quality: RMSE and R^2

Response variable	RMSE	R^2
X-direction accuracy (−)	0.000875	0.4789
Y-direction accuracy (−)	0.0128	0.7375
Z-direction accuracy (−)	0.0172	0.9343
Density (g/cm^3)	0.01776	0.8472
Surface roughness, Ra (μm)	1.3807	0.2960
Elastic modulus (MPa)	86.7118	0.9645
Tensile strength at yield (MPa)	1.5953	0.9615
Nominal strain at break (%)	0.2212	0.9237
Normalized manufacturing time (−)	8.11E-6	1.0000

www.manaraa.com

Overall, GP model training resulted in good model quality. Considering this is the first-time supervised learning with GP is applied to polymer composite materials manufactured by SLS, the results are essential to provide a more in-depth mapping of the influence of the main laser sintering variables over important quality parameters. The model response surfaces are discussed in the next sections.

3.2 Response surfaces

Response surfaces obtained after GP model training for PA12-CF. A given response variable is a function of the three input variables: laser power, laser scan speed, scan line spacing. The multiple input variables result in a hyperplane in a 4-dimensional space that cannot be graphically presented with all variables. To be able to represent the response surfaces of the output variables graphically, three-dimensional intersection plots of this hyperplane are given, with two input variables in the *x*- and *y*-axis and one output variable in the *z*-axis. The remaining input variable is fixed at the given hyperplane. For each output variable evaluated, two three-dimensional graphs are presented: response surface as a function of laser power and laser scan speed at constant scan line spacing; response surface as a function of scan line spacing and laser scan speed at constant laser power.

3.2.1 Dimensional accuracy

Figure 3a–b shows the *Y*- and *Z*-direction accuracy response surfaces as a function of laser power and laser scan speed for a scan line spacing of 0.4 mm. *Y*-direction accuracy varies significantly with laser speed, with a positive gradient in the direction of higher laser speeds. Laser power influences with lower relevance *Y*-direction accuracy. Maximum values are reached at 3000 mm/s and 35 W laser power. Above 3000 mm/s, a plateau is formed, with high values of *Y*-direction accuracy (above 0.99). Lowest values for *Y*-direction accuracy were found at a combination of intermediate laser power and low laser speed. *Z*-direction accuracy has a smoother variation in respect to laser power and laser speed, with the lowest values found at low laser speed and high laser power. *Z*-direction accuracy improves in the direction towards high laser speed and low laser power, reaching a maximum of 0.95 at 25 W laser power and 5000 mm/s laser speed.

Response surfaces for *Y*- and *Z*-direction accuracy as a function of laser speed and scan line spacing for 35 W laser power are depicted in Fig. 3c–d. Values as low as 0.92 are found at low scan speed and scan line spacing, steeply increasing in the direction of higher laser speed and scan line spacing. Both variables have a strong influence on *Y*-direction accuracy. There is a large plateau area where stable *Y*-direction accuracy values (above 0.99) are observed. At this plateau, scan line spacing and laser speed have minimal influence. *Z*-direction accuracy presents a clear tendency of low values at low laser speed and low scan line spacing, improving in the direction towards higher scan line spacing and higher laser speed.

The sensitivity of *Y*-accuracy as a function of the evaluated parameters is shown in Fig. 4a. Laser speed has the most significant influence over *Y*-direction accuracy, followed by scan line spacing and at last laser power with the lowest relevance. The relevance of individual laser sintering parameters over *Z*-direction accuracy is shown in Fig. 4b. As expected from the response surfaces, scan line spacing, and laser speed play a significant relevance, whereas *Z*-direction accuracy is less sensitive to laser power.

During the SLS process, the laser energy delivered to the powder bed undergoes radiation absorption by the PA12-CF particles and multiple transmission to neighboring particles. Both PA12 and CF in the form of anthracite have good absorption at the CO_2 laser wavelength of 10.6 μm [26, 27]. The addition of carbon fiber in anthracite form to PA12 improves the thermal conductivity of the powder bed [28], leading to more heat transferred to the surrounding and underlying unsintered powder, worsening dimensional accuracy of the parts. It has been observed by simulation modeling with PA12 and carbon nanotubes (CNTs) that the laser heat affected area is wider and deeper when laser sintering PA12-CNT compared to PA12 [9].

Both accuracy values in *Y*- and *Z*-direction show similar behavior of improved values at lower energy density range. For instance, lower laser speed increases the exposure time the powder bed is subjected to the laser, increasing the laser beam heat-affected area in both *Y*- and *Z*-directions, decreasing accuracy as surrounding particles are consolidated together with the target particles scanned by the laser. Scan line spacing acts similarly but increasing the number of exposures and the overlap degree between laser lines, also contributing to a higher heat-affected area and worsening dimensional accuracy. Higher laser power affects the melt pool width and depth during laser sintering, also impacting heat-affected area and accuracy.

3.2.2 Density and mechanical properties

The density response surface as a function of laser power and laser speed at 0.4 mm scan line spacing is depicted in Fig. 5a. The surface topology shows very low density values of 0.92 g/cm^3 at the highest laser speed and lowest laser power, increasing in the direction of lower laser scan speed and higher laser power. The gradient in laser speed direction is higher than laser power, indicating higher relevance of laser speed. The surface shows a local maximum of 1.04 g/cm^3 at near 3000 mm/s and 25 W laser power. At constant laser power, there is a decrease in density for lower values than 3000 mm/s. Another high density of area 1.02 g/cm^3 at the highest laser

www.manaraa.com

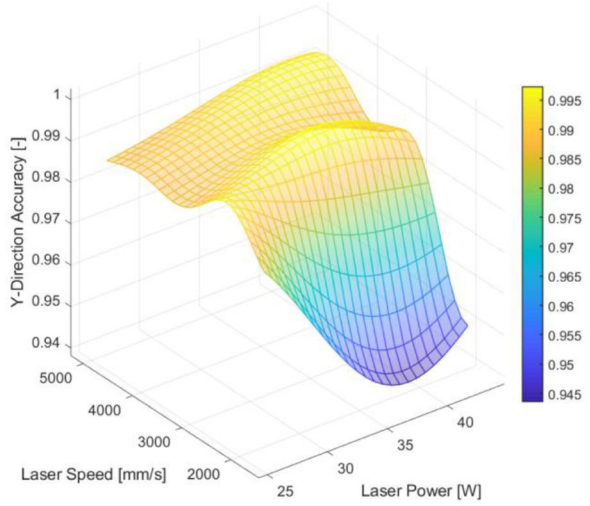

(a) Y-direction accuracy in function of laser speed and laser power for 0.4 mm scan line spacing.

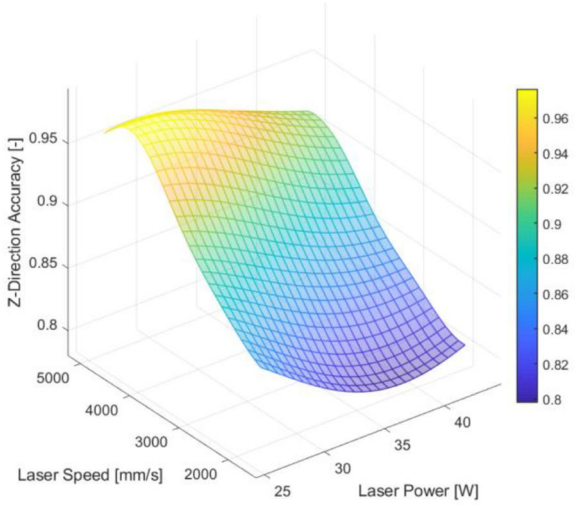

(b) Z-direction accuracy in function of laser speed and laser power for 0.4 mm scan line spacing.

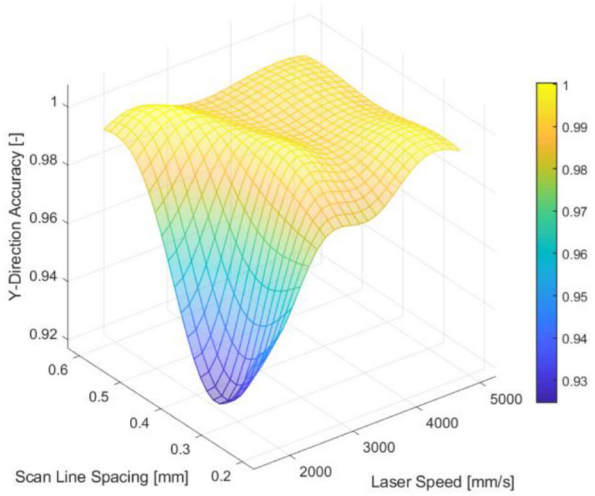

(c) Y-direction accuracy in function of laser speed and scan line spacing for 35 W laser power.

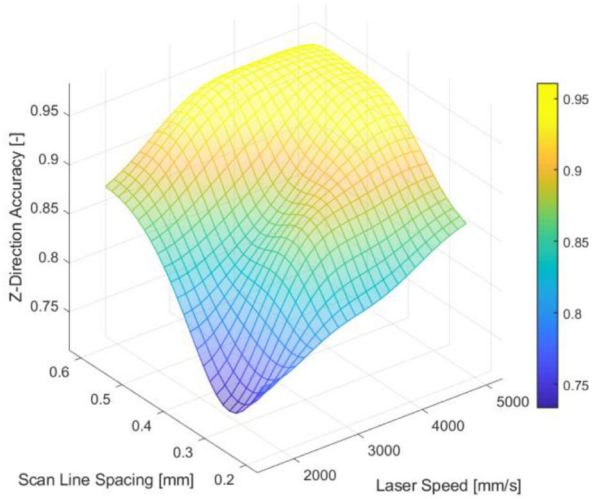

(d) Z-direction accuracy in function of laser speed and scan line spacing for 35 W laser power.

Fig. 3 Response surfaces for dimensional accuracy in *Y*- and *Z*-direction. **a** *Y*-direction accuracy as a function of laser speed and laser power at 0.4 mm scan line spacing. **b** *Z*-direction accuracy as a function of laser speed and laser power at 0.4 mm scan line spacing. **c** *Y*-direction accuracy as a function of laser speed and scan line spacing at 35 W laser power. **d** *Z*-direction accuracy as a function of laser speed and scan line spacing at 35 W laser power

speed of 5000 mm/s and highest laser power. Keeping the gradient in direction to higher laser power and lower laser speed leads to a decrease in density values.

Density response surface as a function of laser speed and scan line spacing at 35 W laser power are shown in Fig. 5b. The map shows the lowest density values of 0.82 g/cm^3 located at high laser speed and scan line spacing, steeply increasing in the direction of lower scan line spacing and laser speed. A maximum large area with density values over 1.03 g/cm^3 is observed at different combinations of low laser speed and high scan line spacing and high laser speed and low scan line spacing. Further decreasing laser speed and scan line spacing leads to a reduction in density values.

The response surface of elastic modulus over laser speed and laser power at 0.4 mm scan line spacing is shown in Fig. 5c. The lowest modulus values of near 3000 MPa are concentrated at 4000 mm/s and 25 W laser power and increase in the direction of both lower laser scan speed and high laser power.

المنارة للاستشارات
www.manaraa.com

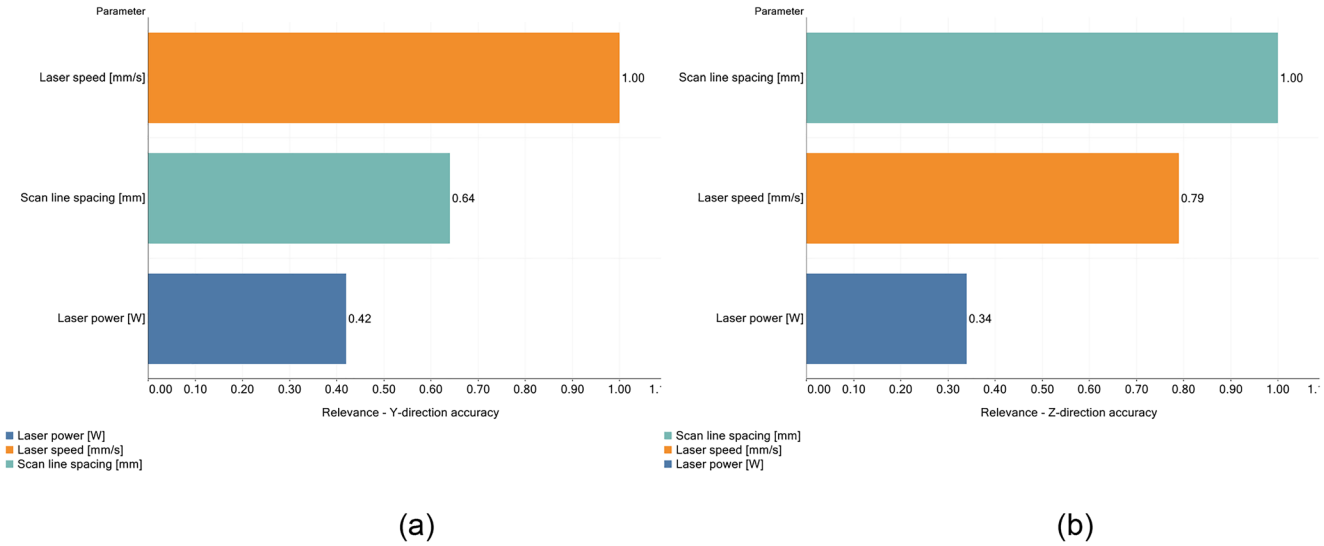

Fig. 4 Sensitivity to SLS process parameters for dimensional accuracy: **a** *Y*-direction and **b** *Z*-direction

Two distinct maximum areas of elastic modulus near 3600 MPa can be observed, one located at an intermediate speed of 3000 mm/s and lowest laser power and the other maximum region located at a maximum laser power of 43 W and 4200 mm/s laser speed. Further increase in laser power combined with lower laser speed results in lower elastic modulus (3300 MPa). Similar behavior is found at the lowest laser speed evaluated, regardless of the laser power.

Elastic modulus response surface as a function of laser speed and scan line spacing at 35 W laser power is depicted in Fig. 5d. The lowest elastic modulus of 2400 MPa is found at high scan line spacing and high laser speed values, steeply increasing with a gradient in the direction towards lower scan line spacing and laser speed. Maximum values near 3600 MPa can be found at different sites in the response surface: scan speed close to 3500 mm/s and scan line spacing near 0.3 mm; scan speed close to 3000 mm/s and scan line spacing of 0.6 mm; scan speed of 5000 mm/s and scan line spacing of 0.2 mm. The combination of very low laser power and scan line spacing results in low elastic modulus.

Figure 6a shows the response surface after GP training for yield strength as a function of laser power and laser speed at 0.4 mm. The surface topology is similar to the elastic properties modeled, presenting the lowest yield strength of 45 MPa at 4000 mm/s laser speed and 25 W laser power. At constant laser power, there is a steep increase in yield strength towards lower laser speed values, reaching a maximum of 65 MPa near 3000 mm/s and decreasing at even lower laser speeds. Keeping laser speed constant at nearly 4000 mm/s, increasing laser power improves yield strength significantly, reaching 65 MPa at a maximum laser power of 43 W. At the lower speed area (below 2500 mm/s), a plateau is formed with slightly lower yield strength values at 62 MPa.

Yield strength as a function of laser speed and scan line spacing at 35 W laser power are depicted in Fig. 6b. Lowest yield strength values (30 MPa) are found at high laser speed and high scan line spacing, steeply increasing in direction to lower laser speed and scan line spacing. A stable plateau with yield strength near 65 MPa is reached in two areas: scan line spacing between 0.4 and 0.6 mm and laser speed below 3000 mm/s; scan line spacing between 0.2 and 0.3 mm and laser speed above 4000 mm/s. Further decrease in both laser speed and scan line spacing reduces yield strength values to 60 MPa.

Nominal strain at break modeled surface as a function of laser power and laser speed at 0.4 mm scan line spacing is depicted in Fig. 6c. The model predicts very low strain at break (3.5%) at low laser power and high laser speed. A gradual transition to increased strain at break values in the direction towards lower laser speed and higher laser power is observed. Maximum values of nominal strain near 5.7% are observed in two regions in the map: laser speed around 4500 mm/s and laser power at 43 W; laser speed at 2000 mm/s and laser power at 25 W. Apart from these two regions, there is a plateau in the high laser power low laser speed area with slightly lower nominal strain at break values (near 5.3%).

Figure 6d shows the response surface of nominal strain at break over laser speed and scan line spacing at 35 W laser power. Surface topology is similar to that found for yield strength, exhibiting lower values of nominal strain at high laser speed and scan line spacing and steeply increasing in direction to lower laser speed and scan line spacing. A plateau is reached in the areas of low laser speed and high scan line spacing and high laser speed and low scan line spacing. Continuous decrease of laser speed below 3000 mm/s and scan line spacing below 0.35 mm slightly reduces nominal strain to values near 5%.

www.manaraa.com

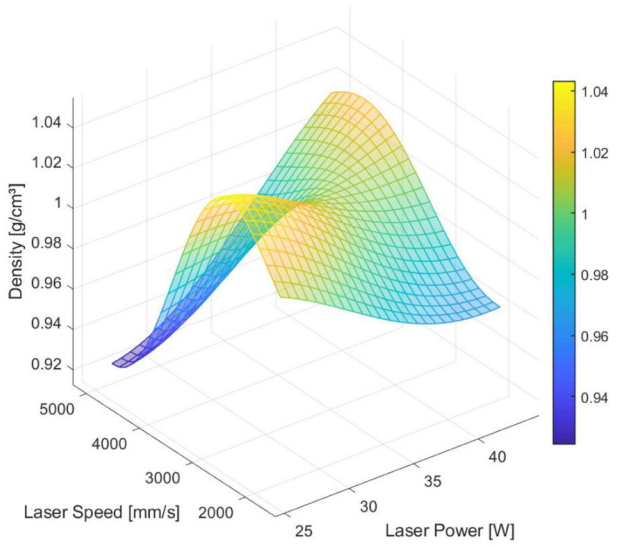

(a) Density in function of laser speed and laser power at 0.4 mm scan line spacing.

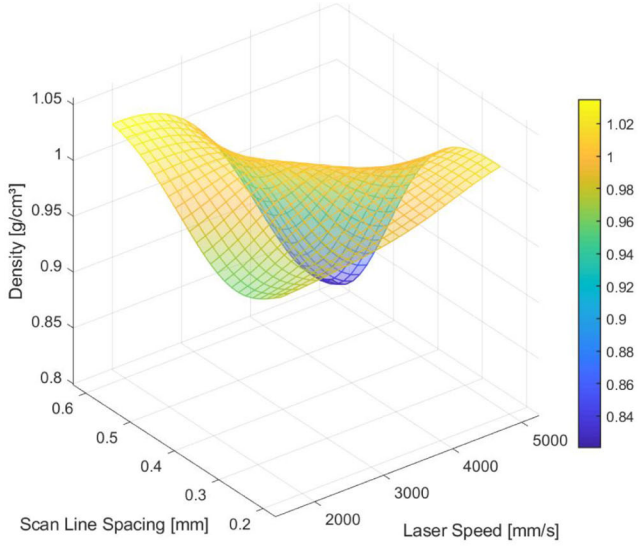

(b) Density in function of laser speed and scan line spacing at 35 W laser power.

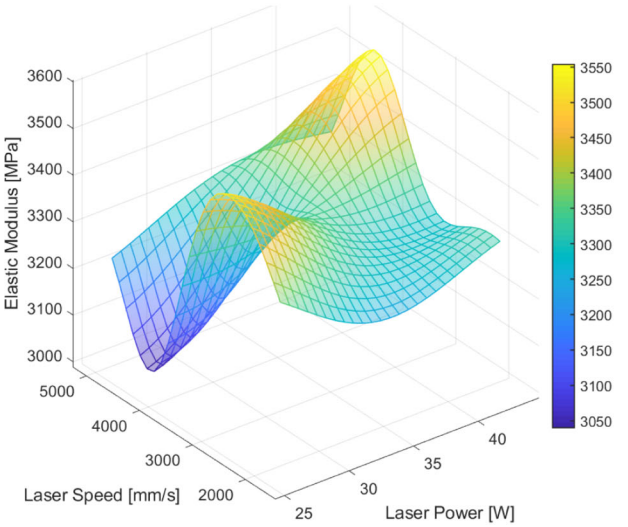

(c) Elastic modulus in function of laser speed and laser power at 0.4 mm scan line spacing.

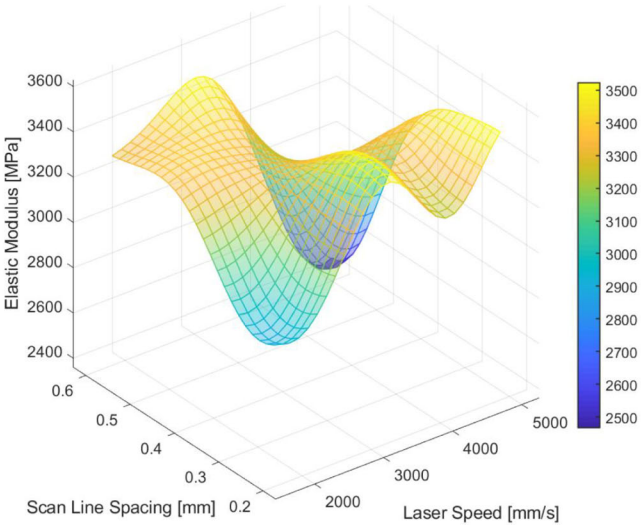

(d) Elastic modulus in function of laser speed and scan line spacing at 35 W laser power.

Fig. 5 Response surfaces for density and elastic modulus. **a** Density as a function of laser speed and laser power at 0.4 mm scan line spacing. **b** Density as a function of laser speed and scan line spacing at 35 W laser power. **c** Elastic modulus as a function of laser speed and laser power at 0.4 mm scan line spacing. **d** Elastic modulus as a function of laser speed and scan line spacing at 35 W laser power

Sensitivity analysis for density and mechanical properties are depicted in Fig. 7a–d. Scan line spacing is the most influencing parameter on density (Fig. 7a) and nominal strain at break (Fig. 7d), followed by laser speed, which has a slightly more substantial relative influence on density compared to nominal strain at break. Density and nominal strain at break are less sensible to laser power. Nevertheless, it is a significant parameter for both response variables. Elastic modulus and yield strength have very similar behavior, being influenced more strongly by laser speed, followed by scan line spacing and, to a less extent, laser power.

SLS is a highly complex process where a combination of factors influence porosity formation and density. Material characteristics such as particle shape and distribution play an essential role in the packing density of the powder bed. PA12 particles have "potato" shape

www.manaraa.com

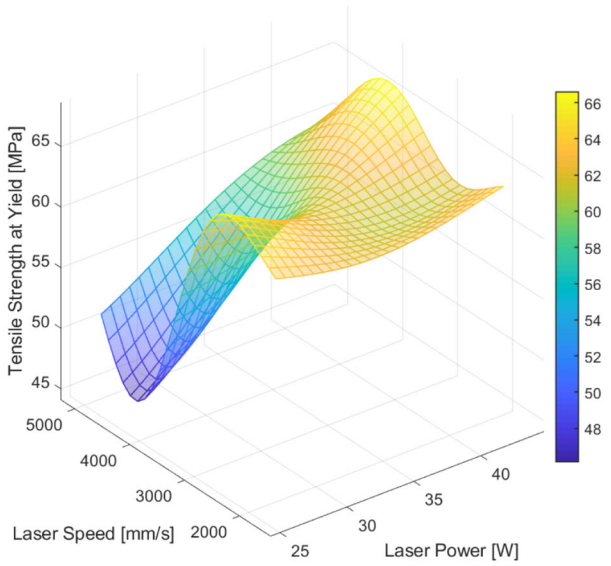

(a) Yield strength in function of laser speed and laser power at 0.4 mm scan line spacing.

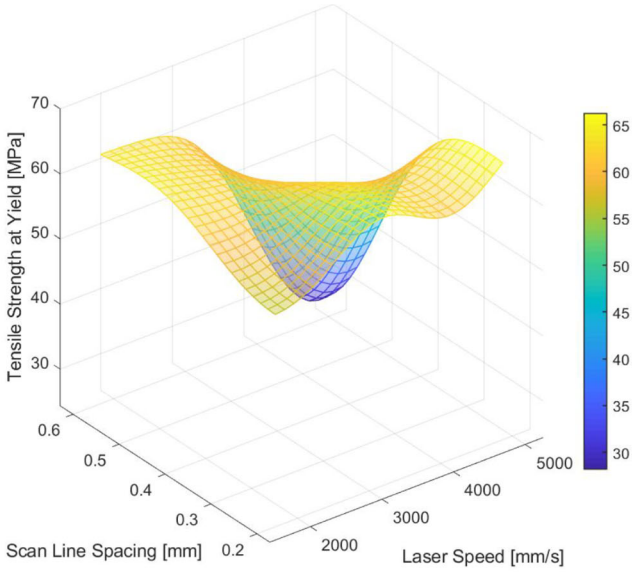

(b) Elastic modulus in function of laser speed and scan line spacing at 35 W laser power.

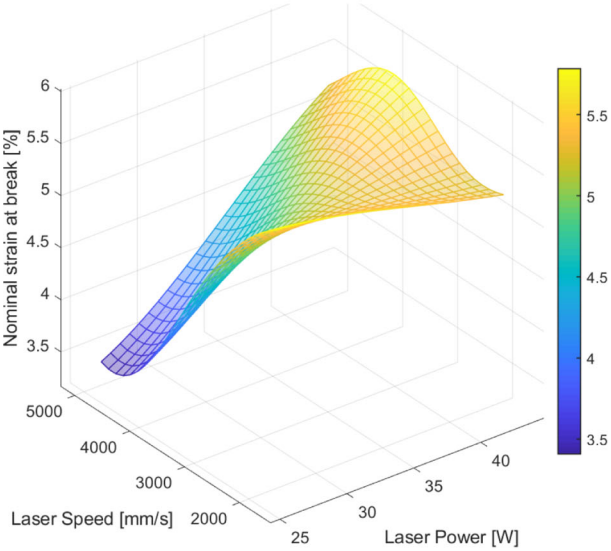

(c) Nominal strain at break in function of laser speed and laser power at 0.4 mm scan line spacing.

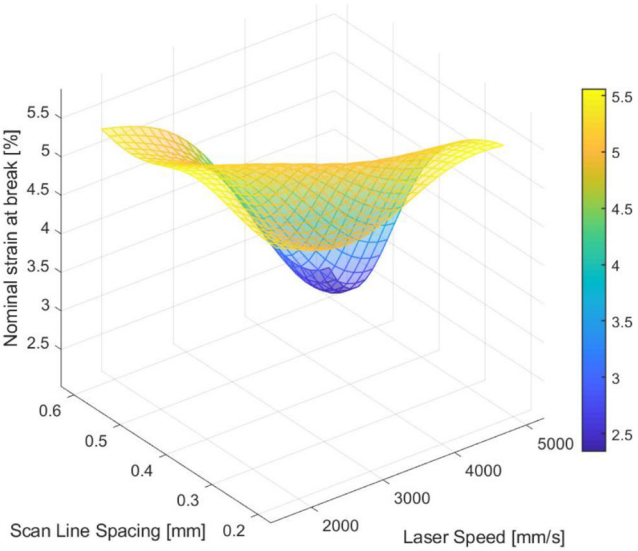

(d) Nominal strain at break in function of laser speed and scan line spacing at 35 W laser power.

Fig. 6 Response surfaces for yield strength and nominal strain at break. **a** Yield strength as a function of laser speed and laser power at 0.4 mm scan line spacing. **b** Elastic modulus as a function of laser speed and scan line spacing at 35 W laser power. **c** Nominal strain at break as a function of laser speed and laser power at 0.4 mm scan line spacing. **d** Nominal strain at break as a function of laser speed and scan line spacing at 35 W laser power

morphology and an adequate particle size distribution, which favors powder spreading and flowability during the SLS process. Carbon fibers present in the PA12 matrix affect the powder spreading over the platform due to their high aspect ratio, causing voids in the packed powder, leading to porosity after SLS consolidation [11]. From laser sintering perspective, the very short laser material interaction during SLS leads to the primary consolidation mechanism of PA12-CF powders via particle rearrangement phase during liquid phase sintering (LPS), where the liquid phase (PA12) flows around the solid particles (CF) via capillary forces [29].

www.manaraa.com

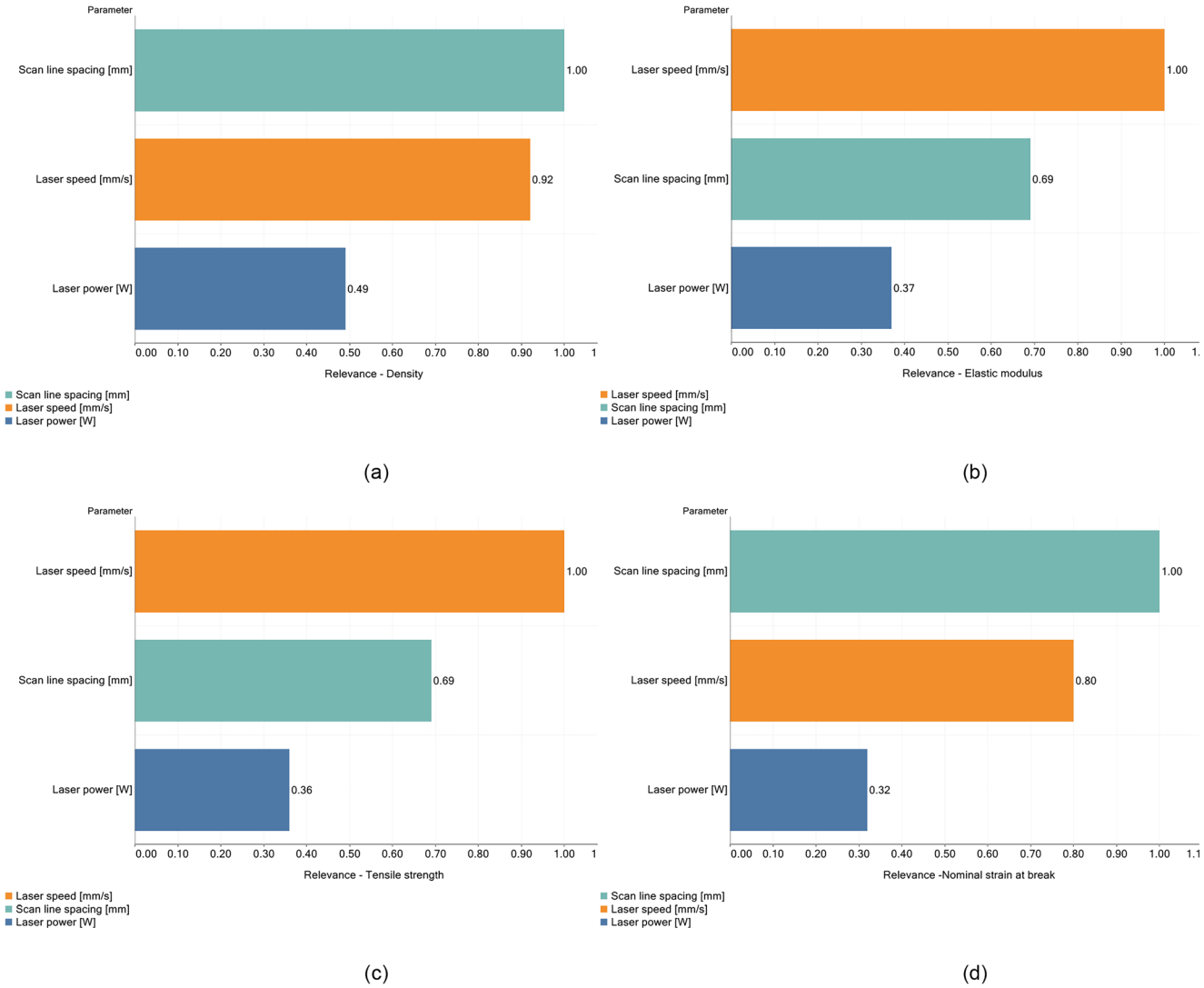

Fig. 7 Sensitivity to SLS process parameters for **a** density, **b** elastic modulus, **c** yield strength, and **d** nominal strain at break

Laser sintering parameters significantly affect the rearrangement phase during LPS and resulting density. The Gaussian process model trained could capture the behavior observed over the individual laser sintering parameters. For instance, higher laser speed decreases the laser material interaction time, reducing the time liquid molten PA12 has to surround CF particles, decreasing the rearrangement phase kinetic force, and leading to lower density. At the same time, this can be compensated with lower scan line spacing and higher overlap degree so that the number of total exposures the same area has is increased, improving sintering dynamics. An increase in laser power to keep the same energy level delivered to the powder bed, but such an approach may not be the most effective due to the lower sensibility density has over laser power. The model also shows the complexity of the individual parameters to achieve optimal density response. The simple decrease of laser speed and scan line spacing or increase in laser power leads to a reduction in density as more energy delivered to the powder bed leads to volume increase due to the consolidation of neighboring particles not scanned by the laser beam as well as polymer degradation.

The mechanical behavior of polymer composites depends on the homogeneity of filler dispersion on the matrix and the adhesion between filler and polymer matrix. The consolidation mechanism by liquid phase sintering mechanism plays an important role in the homogeneity of filler dispersion and adhesion at the matrix-filler interface [30]. The GP model described well the elastic modulus of PA12-CF. At low laser power and high laser speed or high scan line spacing, liquid phase sintering is reduced due to the low liquid content flowing around the filler solid particles. The poor rearrangement phase during LPS leads to weak adhesion between filler and matrix and lower elastic properties.

The GP model also captures the complex trade-offs existing between the individual laser sintering parameters to achieve a combination of low porosity and adequate adhesion

www.manaraa.com

between carbon filler and PA12 matrix. The specific laser sintering parameters necessary to achieve this goal cover a wide area of the design space. For instance, the individual use of high laser speed promotes poor sintering conditions as there is no time for effective liquid formation and presence for a prolonged time. However, the use of high laser speed and low scan line spacing reduces the exposure time while increases the number of laser exposures, providing more time for the rearrangement phase during liquid phase sintering to occur. The use of low laser power associated with a low laser speed achieves a similar behavior. The GP model describes adequately the decrease in mechanical properties towards very low laser speed and scan line spacing or low laser speed and high laser power, resulting in a high-energy density applied. The decrease in elastic modulus and yield strength at these sintering parameters is associated with a reduction in PA12 crystal fraction present after consolidation [31, 32]. The impact is more significant on elastic properties compared to plastic properties, as observed from the smoother surface topology of yield strength and nominal strain at break compared to elastic modulus response variables. Nominal strain at break initially improves from the higher energy laser sintering parameters applied, as the plastic strain on PA12-CF results from the deformation of amorphous chains located in the PA12 matrix. At very high-energy densities, polymer degradation is the governing mechanism responsible for the reduction in mechanical properties, as already observed by other authors when processing PA12-CF [10].

3.2.3 Normalized manufacturing time

Figure 8a shows the normalized manufacturing time response surface as a function of laser power and laser speed at 0.4 mm scan line spacing. Normalized manufacturing time varies almost linearly with laser speed, with the lowest values at high laser speed and increasing in the direction of lower laser speed. This behavior is in agreement with the SLS process, as the laser speed influences the time required to scan the powder bed, with higher laser speed requiring less time than lower laser speed to scan over the same powder bed surface. However, the reduction in time is not of grand scale, with a maximum reduction in 3% observed at the highest laser speed applied. Laser power does not influence significantly normalized manufacturing time.

Normalized manufacturing time over laser speed and scan line spacing at 35 W laser power are depicted in Fig. 8b. The model shows a smooth surface with the lowest manufacturing time of 0.965 at the highest laser speed and scan line spacing, increasing in the direction towards low laser speed and scan line spacing. Maximum values of 1.04 are found at the lowest laser speed and scan line spacing evaluated.

As shown in Fig. 9, scan line spacing has the highest influence on normalized manufacturing time, closely followed by laser speed. As expected, normalized manufacturing time is not influenced by laser power.

3.3 Stochastic optimization through evolutionary algorithm

After successful learning of the training data via GP, several multi-objective optimization tasks were conducted using EA. As the model quality for surface roughness was not adequate, the optimization tasks involving minimizing surface roughness were not considered, and the optimization was conducted for mechanical properties, dimensional accuracy, and manufacturing time (criteria 1, 3, and 6).

3.3.1 Criterion 1—Optimization of manufacturing time and dimensional accuracy

Criterion 1 seeks the optimization of manufacturing time and dimensional accuracy while keeping mechanical properties at acceptable values. In order to perform this task, mechanical properties were set as hard upper limits, meaning that optimization solutions that result in mechanical properties lower than the thresholds set as hard upper limits will be discarded. Yield strength was set as hard upper bound at 59 MPa, elastic modulus at 3276 MPa, and nominal strain at break at 4.87%.

Figure 10a depicts the Pareto solutions for *Z*-direction accuracy and normalized manufacturing time after the optimization task with criterion 1. The maximum accuracy achieved is 0.94, while minimum normalized manufacturing time is 0.97. Two Pareto sets were chosen from all solutions at the Pareto frontier: Pareto set 1 shows lowest values for normalized manufacturing time (0.97) and good *Z*-direction accuracy around 0.937; Pareto set 2 has slightly better values for *Z*-direction accuracy (near 0.94) at the cost of higher normalized manufacturing time (0.976–0.977). The first Pareto set chosen a better solution set for the optimization task; nevertheless, solution set 2 was chosen for comparison as well.

The laser sintering parameters at the Pareto frontier can be observed in Fig. 10b. Pareto set 1 laser sintering parameters are clustered at higher laser power are between 42 and 43 W, high laser speed area between 4300 and 4500 mm/s, and scan line spacing between 0.43 and 0.44 mm. Pareto solution set 2 gives an entirely different scenario of lower laser power at 33 W, lower laser speed near 2800 mm/s, and very high scan line spacing at 0.57 mm. Pareto set 1 gives better results in terms of normalized manufacturing time as the laser speed applied is much higher than Pareto set 2.

3.3.2 Criterion 3—Optimization of dimensional accuracy and mechanical properties

Multi-objective optimization task with criterion 3 aims the maximization of dimensional accuracy and mechanical

www.manaraa.com

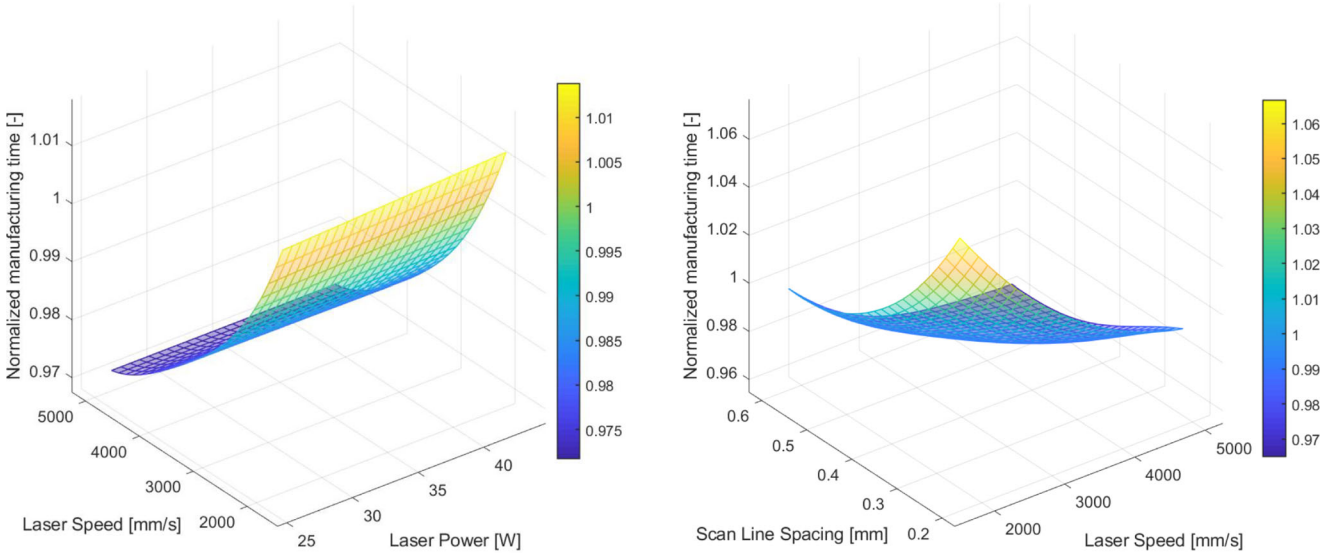

(a) Normalized manufacturing time in function of laser power speed 0.4 mm scan line spacing.

(b) Normalized manufacturing time in function of laser speed and scan line spacing at 35 W laser power.

Fig. 8 Response surfaces for normalized manufacturing time. **a** Normalized manufacturing time as a function of laser power speed 0.4 mm scan line spacing. **b** Normalized manufacturing time as a function of laser speed and scan line spacing at 35 W laser power

properties. All main mechanical properties outputs (elastic modulus, yield strength, and nominal strain at break) were maximized as well as dimensional accuracy in all directions. Normalized manufacturing time was set as hard upper bound at 0.99.

Figure 11a shows the Pareto frontier for yield strength and nominal strain at break over *Z*-direction accuracy. A well-defined Pareto frontier is observed, and the trade-off solutions between mechanical properties and dimensional accuracy are visible. Dimensional accuracy and mechanical properties are conflicting objective functions, so the choice of parameters must be carefully observed. To perform the analysis, three Pareto solution sets were chosen: first Pareto set focused on high mechanical properties (yield strength above 68 MPa) in detriment of lower dimensional accuracy (between 0.91 and 0.92); Pareto group 2 allowed slightly lower yield strength (below 67 MPa) values to improve dimensional accuracy (*Z*-direction accuracy between 0.93 and 094); Pareto set 3 focused on maximum *Z*-direction accuracy values (above 0.97) at the cost of much lower mechanical properties (yield strength between 50 and 51 MPa); Pareto set 4 was chosen in order to maximize nominal strain at break values, which do

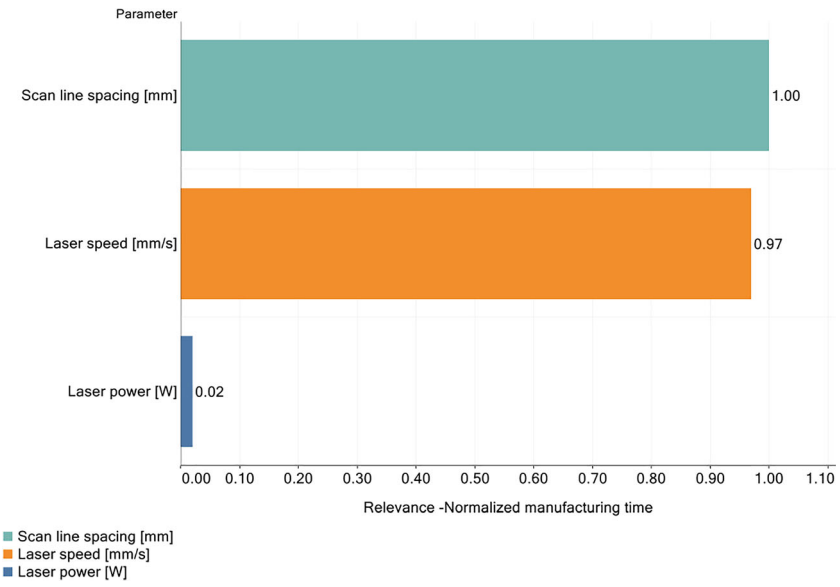

Fig. 9 Sensitivity to SLS process parameters for normalized manufacturing time

www.manaraa.com

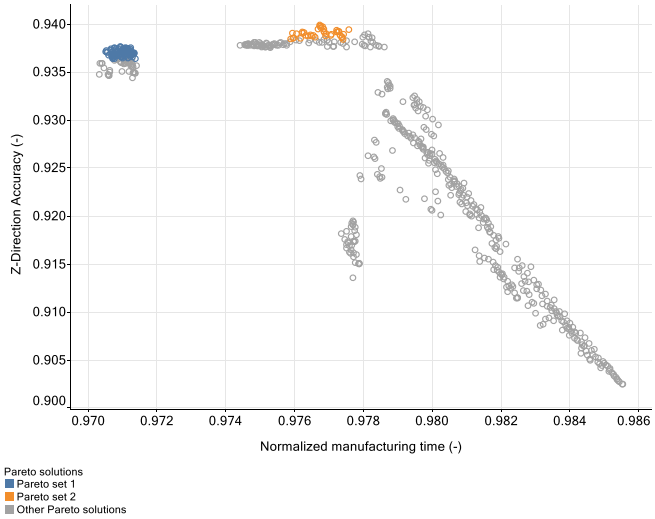

(a) Pareto frontier for optimization criteria 1.

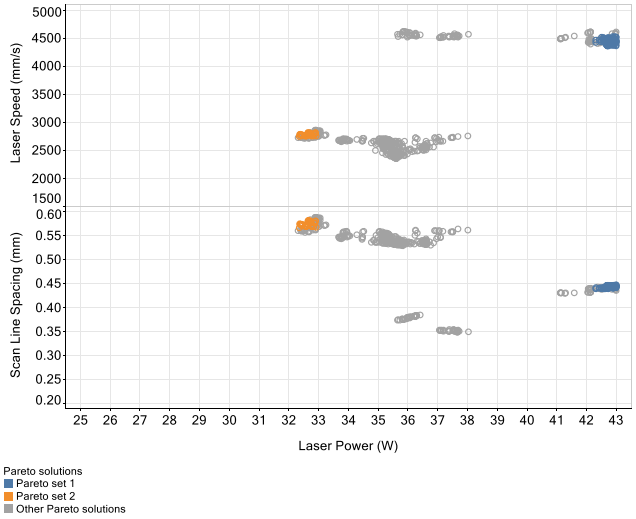

(b) Laser sintering parameters at Pareto frontier for optimization criteria 1.

Fig. 10 Pareto solutions for optimization task with criterion 1. **a** Pareto frontier for optimization criterion 1. **b** Laser sintering parameters at Pareto frontier for optimization criterion 1

not show a direct correlation with yield strength depending on the value range.

Laser speed, scan line spacing, and laser power at the Pareto frontier for criterion 3 are depicted in Fig. 11b. Each Pareto set leads to a different laser sintering parameter combination. At Pareto set 1, laser scan speed solutions are concentrated near 3000 mm/s at a laser power between 41 and 43 W and scan line spacing between 0.56 and 0.6 mm. Pareto set 2 results in similar parameters except that laser speed is higher (above 3300 mm/s) and lower scan line spacing (between 0.55 and 0.57 mm). Pareto set 3 is are grouped in two regions: laser power between 28 and 30 W, laser speed between 4300 and 4600 mm/s and scan line spacing between 0.38 and 0.4 mm; second region occurs at high laser power above 41 W, lower laser speed between 4150 and 4450 mm/s and scan line spacing ranging from 0.5 to 0.52 mm. At last, Pareto set 4 values are concentrated at laser power higher than 40 W, a narrow laser speed area near 4500 mm/s, and scan line spacing between 0.37 and 0.4 mm.

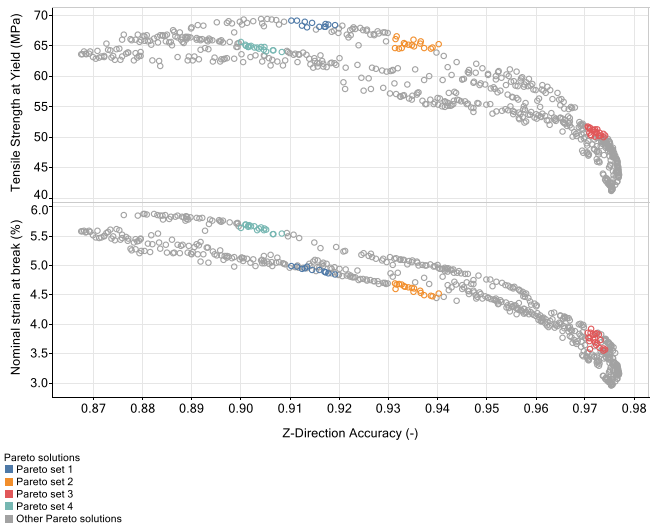

(a) Pareto frontier for optimization criteria 3

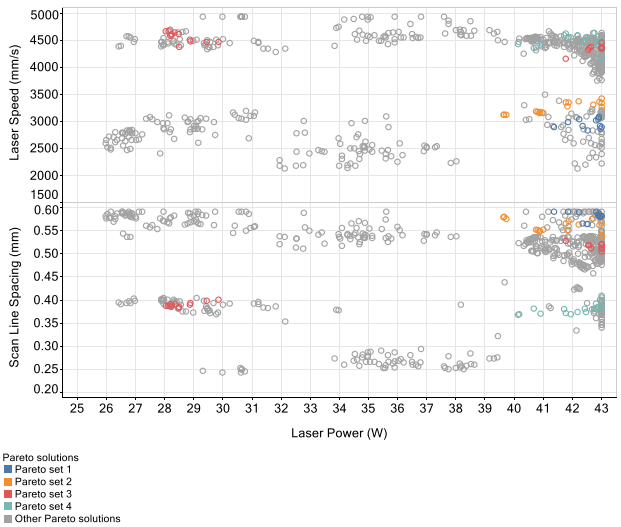

(b) Laser sintering parameters at Pareto frontier for optimization criteria 3

Fig. 11 Pareto solutions for optimization task with criterion 3. **a** Pareto frontier for optimization criterion 3. **b** Laser sintering parameters at Pareto frontier for optimization criterion 3

www.manaraa.com

A closer look at the optimized laser sintering parameters reveals that laser speed values are always attained intermediate to a high level. This result is in agreement with the response surfaces obtained from the GP model, which showed a decrease in mechanical properties at too low laser speed. There is a tendency towards higher laser power when mechanical strength is desired in the Pareto frontier. This tendency was also observed and predicted by the Gaussian model, although high yield strength was also achieved at lower power. Low scan line spacing seems decisive when higher nominal strain at break is desired, whereas higher scan line spacing is higher when yield strength is the focus. The overlapping degree plays an important role here by improving the number of laser exposures of the previously scanned area of the powder bed.

3.3.3 Criterion 6—Optimization of normalized manufacturing time and mechanical properties

The target of the optimization task with criterion 6 is to maximize mechanical properties and normalized manufacturing time. In order to perform the task, also reaching adequate values of dimensional accuracy and surface roughness, *Y*- and *Z*-direction accuracy were set as hard lower limits at 0.98 and 0.88, respectively.

Figure 12a shows the Pareto frontier after EA optimization for criterion 6. The curve shows a well-defined Pareto frontier with clear trade-off values. Three Pareto sets were evaluated: Pareto set 1 is focused on mechanical properties optimization with normalized manufacturing time below 0.98; Pareto set 2 is similar to Pareto set 1 but has lower yield strength target values (between 64 and 66.6 MPa) with highest nominal strain at break and lower range for normalized manufacturing time; Pareto set 3 has much softer values of yield strength (44–46 MPa) and nominal strain at break (3.54 %) with the benefit of lower normalized manufacturing time (0.965).

Laser sintering parameters at Pareto frontier are shown in Fig. 12b. A different set of SLS parameters is achieved depending on the specific trade-off desired. Pareto set 1 aims highest yield strength, resulting in optimized parameters clustered at high laser power (43 W), intermediate laser speed between 2500 and 2800 mm/s, and high scan line spacing at 0.6 mm. Pareto set 2 is focused on achieving the highest nominal strain, leading to higher laser speed values between 4000 and 4500 mm/s and lower scan line spacing between 0.35 and 0.41 mm while keeping the same laser power level near 43 W. Pareto set 3 seeks lowest normalized manufacturing time. Therefore, highest laser speed is desired (5000 mm/s) combined to higher scan line spacing at 0.5 mm and high laser power. Comparing Pareto sets 2 and 3, it can be observed that a small increase in laser speed and scan line spacing promotes a significant reduction in mechanical properties (30% reduction in yield strength and 40% in strain at break) at the cost of a small decrease in normalized manufacturing time (1%).

4 Conclusions

This work investigated the influence of the individual laser sintering parameters on the mechanical and dimensional properties of SLS produced PA12-CF samples. For the first time, response surface modeling via Gaussian process (GP)–

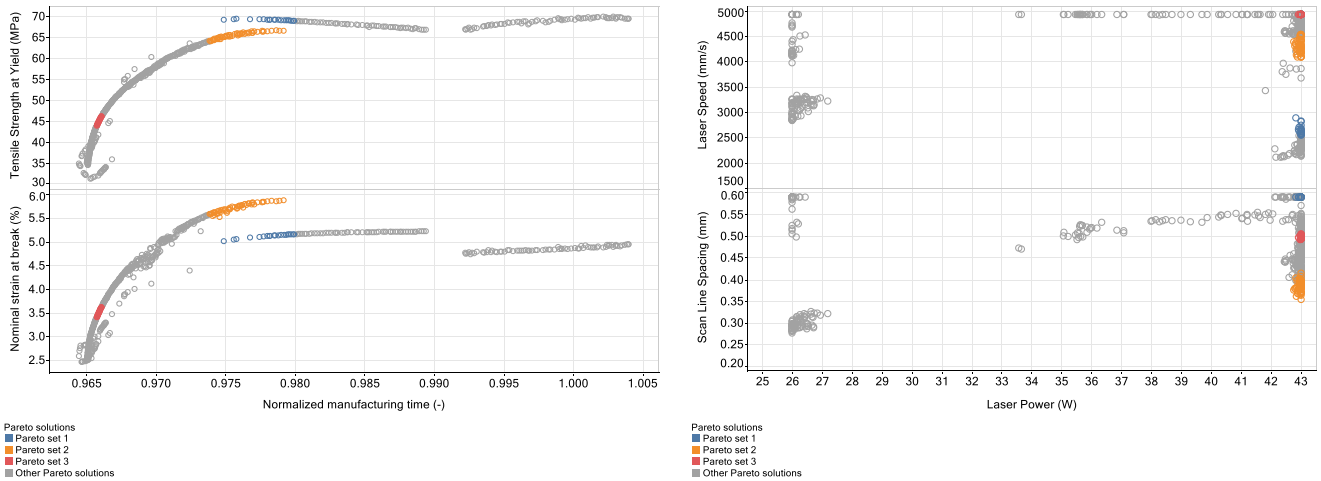

(a) Pareto frontier for optimization criteria 6.

(b) Laser sintering parameters at Pareto frontier for optimization criteria 6.

Fig. 12 Pareto solutions for optimization task with criterion 6. **a** Pareto frontier for optimization criterion 6. **b** Laser sintering parameters at Pareto frontier for optimization criterion 6

www.manaraa.com

supervised learning was successfully employed, covering a wide range of laser sintering parameters and providing more in-depth information on the influence of individual laser sintering parameters over important quality variables. At last, multi-objective stochastic optimization employing evolutionary algorithm (EA) was deployed for both PA12-CF in different criteria scenarios, aiming to understand the behavior of individual laser sintering parameters when subjected to several optimization tasks. The following conclusions can be drawn:

- Excellent model quality (adequate for quantitative assessment) was achieved for the following output variables: *Z*-direction accuracy, density, yield strength, nominal strain at break, elastic modulus, and normalized manufacturing time.
- Intermediate model quality (adequate for qualitative assessment) was achieved for the following output variables: density, *Y*-direction accuracy.
- Response surfaces showed a wide variation of topologies depending on the response variable, many of which with a highly non-linear shape. The GP could successfully capture the non-linear effects and provide detailed information on the correlation of laser sintering parameters and output variables, which can be used for both prediction and optimization of process variables.
- The relevance of individual laser sintering parameters depends strongly on the related response variable evaluated. There is no individual parameter with the highest overall relevance that could be ranked, although laser power had the lowest significance among the parameters evaluated.
- Laser sintering parameters at optimized Pareto frontier vary to a great extent depending on the trade-off objective desired and the criteria used for optimization.
- Optimization of manufacturing time and dimensional accuracy led to Pareto sets clustered at high laser power, high laser speed, and medium to high scan line spacing or intermediate laser power and laser speed and high scan line spacing.
- Optimization of mechanical properties and dimensional accuracy led to optimized laser sintering parameters clustered mainly at high laser power and intermediate to high laser speed. Scan line spacing varied from intermediate to high values. A clear difference was observed in Pareto sets maximizing strain at break or yield strength.
- Optimization of mechanical properties and manufacturing time resulted in Pareto solutions clustered at high laser power and intermediate to high values for laser speed and scan line spacing values, depending on the desired trade-off solution.

Funding This study is financially supported by Financiadora de Estudos e Projetos (FINEP).

Compliance with ethical standards

Conflict of interest The authors declare that they have no conflict of interest.

References

1. Kruth JP, Wang X, Laoui T, Froyen L (2003) Lasers and materials in selective laser sintering. Assem Autom 23:357–371. https://doi.org/10.1108/01445150310698652
2. ASTM Standard F2792-12a (2012) Standard Terminology for additive manufacturing technologies. West Conshohocken, PA
3. Kruth J-P, Mercelis P, van Vaerenbergh J, Froyen L, Rombouts M (2005) Binding mechanisms in selective laser sintering and selective laser melting. Rapid Prototyp J 11:26–36. https://doi.org/10.1108/13552540510573365
4. Wang X, Jiang M, Zhou Z, Gou J, Hui D (2017) 3D printing of polymer matrix composites: a review and prospective. Compos Part B 110:442–458. https://doi.org/10.1016/J.COMPOSITESB.2016.11.034
5. Goodridge RD, Tuck CJ, Hague RJM (2012) Laser sintering of polyamides and other polymers. Prog Mater Sci 57:229–267. https://doi.org/10.1016/j.pmatsci.2011.04.001
6. van de Werken N, Tekinalp H, Khanbolouki P, Ozcan S, Williams A, Tehrani M (2020) Additively manufactured carbon fiber-reinforced composites: state of the art and perspective. Addit Manuf 31:100962. https://doi.org/10.1016/j.addma.2019.100962
7. Kumar S, Kruth JP (2010) Composites by rapid prototyping technology. Mater Des 31:850–856. https://doi.org/10.1016/j.matdes.2009.07.045
8. Yan C, Hao L, Xu L, Shi Y (2011) Preparation, characterisation and processing of carbon fibre/polyamide-12 composites for selective laser sintering. Compos Sci Technol 71:1834–1841. https://doi.org/10.1016/j.compscitech.2011.08.013
9. Bai J, Goodridge RD, Yuan S, Zhou K, Chua C, Wei J (2015) Thermal influence of CNT on the polyamide 12 nanocomposite for selective laser sintering. Molecules 20:19041–19050. https://doi.org/10.3390/molecules201019041
10. Jing W, Hui C, Qiong W, Hongbo L, Zhanjun L (2017) Surface modification of carbon fibers and the selective laser sintering of modified carbon fiber/nylon 12 composite powder. Mater Des 116:253–260. https://doi.org/10.1016/j.matdes.2016.12.037
11. Jansson A, Pejryd L (2016) Characterisation of carbon fibre-reinforced polyamide manufactured by selective laser sintering. Addit Manuf 9:7–13. https://doi.org/10.1016/j.addma.2015.12.003
12. Liu Y, Zhu L, Zhou L, Li Y (2019) Microstructure and mechanical properties of reinforced polyamide 12 composites prepared by laser additive manufacturing. Rapid Prototyp J 25:1127–1134. https://doi.org/10.1108/RPJ-08-2018-0220
13. Salmoria GV, Paggi RA, Lago A, Beal VE (2011) Microstructural and mechanical characterization of PA12/MWCNTs nanocomposite manufactured by selective laser sintering. Polym Test 30:611–615. https://doi.org/10.1016/j.polymertesting.2011.04.007
14. Goodridge RD, Shofner ML, Hague RJM, McClelland M, Schlea MR, Johnson RB, Tuck CJ (2011) Processing of a polyamide-12/carbon nanofibre composite by laser sintering. Polym Test 30:94–100. https://doi.org/10.1016/j.polymertesting.2010.10.011
15. Espera A, Palaganas J, Chen Q et al (2019) 3D printing of a robust polyamide-12-carbon black composite via selective laser sintering: thermal and electrical conductivity OLED preparation and surface initiated polymerization view project 3D printing of covalent functionalized graphene oxide nanocomposite via stereolithography view project 3D printing of a robust polyamide-12-carbon black

www.manaraa.com

composite via selective laser sintering: thermal and electrical conductivity. Macromol Mater Eng. https://doi.org/10.1002/mame.201800718
16. Hong R, Zhao Z, Leng J, Wu J, Zhang J (2019) Two-step approach based on selective laser sintering for high performance carbon black/ polyamide 12 composite with 3D segregated conductive network. Compos Part B 176:107214. https://doi.org/10.1016/j.compositesb.2019.107214
17. Zhu W, Yan C, Shi Y, Wen S, Liu J, Wei Q, Shi Y (2016) A novel method based on selective laser sintering for preparing high-performance carbon fibres/polyamide12/epoxy ternary composites. Sci Rep 6:1–10. https://doi.org/10.1038/srep33780
18. EOS (2020) Material data center. http://eos.materialdatacenter.com/eo/en. Accessed 9 Jan 2020
19. ASTM Standard D638-02a (2002) Standard test method for tensile properties of plastics. West Conshohocken
20. ASTM Standard D790-02 (2002) Standard test methods for flexural properties of unreinforced and reinforced plastics and electrical insulating materials. West Conshohocken
21. Cavazzuti M (2013) Optimization methods: from theory to design. Springer-Verlag, Berlin Heidelberg
22. Rasmussen CE, Williams CKI (2006) Rasmussen and Williams - Gaussian processes for machine learning
23. Rasmussen CE (2020) Web page. http://www.gaussianprocess.org/gpml/code/matlab/doc/. Accessed 19 Oct 2019
24. Storn RM, Kenneth P (1997) Differential evolution - a simple and efficient adaptive scheme for global optimization over continuous spaces. J Glob Optim 11:341–359. https://doi.org/10.1023/A:1008202821328
25. ASTM Standard D5947-11 (2012) Standard test methods for physical dimensions of solid plastics specimens
26. Laumer T, Stichel T, Nagulin K, Schmidt M (2016) Optical analysis of polymer powder materials for selective laser sintering. Polym Test 56:207–213. https://doi.org/10.1016/j.polymertesting.2016.10.010
27. Ribeiro N, Mattos D, Rodrigues C et al (2018) Azo dye adsorption on anthracite: a view of thermodynamics, kinetics and cosmotropic effects. Sep Purif Technol 209:806–814. https://doi.org/10.1016/j.seppur.2018.09.027
28. Herrin JM, Deming D (1996) Thermal conductivity of U.S. coals. J Geophys Res Solid Earth 101:25381–25386. https://doi.org/10.1029/96jb01884
29. Anestiev L, Froyen L (1999) Model of the primary rearrangement processes at liquid phase sintering and selective laser sintering due to biparticle interactions. J Appl Phys 86:4008–4017. https://doi.org/10.1063/1.371321
30. Kruth J-P, Levy G, Klocke F, Childs THC (2007) Consolidation phenomena in laser and powder-bed based layered manufacturing. CIRP Ann Manuf Technol 56:730–759. https://doi.org/10.1016/j.cirp.2007.10.004
31. Jauffrès D, Lame O, Vigier G, Doré F, Douillard T (2009) Sintering mechanisms involved in high-velocity compaction of nascent semi-crystalline polymer powders. Acta Mater 57:2550–2559. https://doi.org/10.1016/j.actamat.2009.02.012
32. Dupin S, Lame O, Barrès C, Charmeau J-YY (2012) Microstructural origin of physical and mechanical properties of polyamide 12 processed by laser sintering. Eur Polym J 48:1611–1621. https://doi.org/10.1016/j.eurpolymj.2012.06.007

Publisher's note Springer Nature remains neutral with regard to jurisdictional claims in published maps and institutional affiliations.

المنارة للاستشارات
www.manaraa.com

Reproduced with permission of copyright owner. Further reproduction prohibited without permission.

www.manaraa.com